LARS Information Note 022283

EVALUATION OF THE RADIOMETRIC QUALITY OF THE TM DATA USING CLUSTERING, LINEAR TRANSFORMATIONS AND MULTISPECTRAL DISTANCE MEASURES

By

L.A. Bartolucci

M.E. Dean

P.E. Anuta

Laboratory for Applications of Remote Sensing

Purdue University

West Lafayette, Indiana

February 22, 1983

In Proceedings, Landsat-4 Scientific Characterization Early Results Symposium, NASA Goddard Space Flight Center, Greenbelt, MD 20771, February 22-24, 1983.

EVALUATION OF THE RADIOMETRIC QUALITY OF THE TM DATA USING CLUSTERING, LINEAR TRANSFORMATIONS AND MULTISPECTRAL DISTANCE MEASURES

by

L.A. Bartolucci[1], M.E. Dean[2] and P.E. Anuta[3]
Laboratory for Applications of Remote Sensing
Purdue University

INTRODUCTION

For the past ten years the remote sensing research community and users of space-acquired multispectral scanner data have developed and applied successfully a variety of digital techniques to extract useful information from the Landsat MSS data for mapping, inventorying, monitoring, and managing the earth resources.

Now with the availability of the Thematic Mapper (TM) data, different analysis techniques will be required to deal with the improved spatial and spectral resolutions, and with the higher dimensionality and sensitivity of the TM data.

The primary objective of this investigation was to evaluate the radiometric quality of the TM data for classification and identification of earth surface features utilizing clustering, data compression (linear transformations), multispectral distance measures, and hierarchical classification techniques.

COMPARISON BETWEEN "A"-TAPE AND "P"-TAPE TM DATA

For this investigation, the three different types of TM data tapes were requested, i.e. B-tapes (raw data), A-tapes (radiometrically corrected data), and P-tapes (geometrically corrected data) for a number of different test sites. To date, however, only A-tapes and P-tapes were received for the Chicago, Illinois and Webster Co., Iowa test sites. The identification information for the TM and MSS data sets used in this investigation is shown in Table 1.

---

[1]Technical Director, Technology Transfer Programs
[2]Graduate Research Assistant
[3]Associate Program Leader, Data Processing and Analysis Research Programs

Table 1. TM and MSS Data Sets (A and P tapes)

Scene ID	Data	Location
40049-16264	9/03/82	Iowa
40101-16025	10/25/82	Illinois

In order to determine the effect of the geometric correction process (resampling - gray level interpretation) on the radiometry of the new resampled pixels when converting the data from an A-tape (30m x 30m pixels) to a P-tape (28.5m x 28.5m pixels) format, the means and standard deviation for homogeneous and heterogeneous areas on the ground were calculated using the data from both the A and P-tapes. A comparison of both sets of statistics, illustrated in Tables 2 and 3, demonstrate that there has not been a significant change (radiometric degradation) caused by the non-zero-order (cubic convolution) interpolation process.

Furthermore, in order to determine whether the cubic convolution interpolation had affected the structure of the data in feature space, a set of data from the A and P-tapes for the same area on the ground were clustered (Ref. 14) into 16 cluster classes. Then, the resulting 16 cluster classes from the A and P data sets were merged together into a single 32 class file. Subsequently, the pair-wise spectral separability for the 32 classes was computed using a Transformed Divergence algorithm (Ref. 12). Table 4 shows the transformed divergence (D_T) measures for all the pairs of corresponding classes from the A and P-tape data sets. For example, the transformed divergence between the second cluster class from the TM A-tape (symbol B) and the corresponding second cluster class from the TM P-tape (symbol R) is 53, and since the transformed measure ranges from zero to 2000 (Ref. 13); where a value of 2000 indicates that the two classes in question are completely separable (different), and any D_T value between zero and 500 indicates that the pair of classes are not separable (very similar), it may be concluded that the 16 cluster classes obtained from the A and P tapes are essentially equivalent. Thus these results corroborate the previously stated conclusion that the radiometry of the resampled pixels from the P-tape have not been significantly affected by the geometric correction process, consequently meeting the GSFC specifications for the Landsat-D system, i.e. 'resampling shall not introduce radiometric degradation of more than 1 quantum level' (Ref. 9). Based on these findings, the rest of the results reported in this paper deal with only the TM P-tape data.

NOTE: Thoughout this paper band 6 refers to the 2.08-2.35 μm band, and band 7 refers to the TM thermal infrared band.

Table 2.

MEANS AND STANDARD DEVIATIONS FOR HOMOGENEOUS AREAS IN THE TM "A" AND "P" DATA SETS (Scene ID: 40049-16264)

Bright Homogeneous Target

TM A-Tape

Band	1	2	3	4	5	6	7
Mean	72.64	33.75	37.93	64.59	119.95	57.23	136.77
St. Dev.	2.27	1.45	2.85	2.49	6.37	3.28	3.74

TM P-Tape

Band	1	2	3	4	5	6	7
Mean	72.88	33.95	38.30	64.34	120.80	*	137.75
St. Dev.	2.18	1.42	2.83	2.52	6.54	*	3.46

* LARS band 6 (2.08-2.35 μ m) had not arrived at the time these calculations were performed.

Table 3.

MEANS AND STANDARD DEVIATIONS FOR HETEROGENEOUS AREAS IN THE TM "A" AND "P" DATA SETS (Scene ID: 40049-16264)

Heterogeneous Area

TM A-Tape

Band	1	2	3	4	5	6	7
Mean	68.31	29.56	26.94	89.58	75.75	27.94	127.78
St. Dev.	15.31	8.91	13.12	21.30	16.35	12.62	4.53

TM P-Tape

Band	1	2	3	4	5	6	7
Mean	68.28	29.56	26.90	89.77	75.92	*	127.83
St. Dev.	15.36	8.94	13.10	21.80	16.42	*	4.65

* LARS band 6 (2.08-2.35 μm) had not arrived at the time these calculations were performed.

Table 4.

SEPARABILITY FOR THE MERGED TM "A" AND "P" TAPE CLUSTER CLASSES

CLASS SYMBOLS				CLASS PAIRS	D_T*
"A" Tape	A	"P" Tape	Q	AQ	59
	B		R	BR	53
	C		S	CS	164
	D		T	DT	85
	E		U	EV	35
	F		V	FU	150
	G		W	GW	60
	H		X	HX	99
	I		Y	IY	108
	J		Z	JZ	262
	K		$	K$	63
	L		+	L+	62
	M		=	M=	22
	N		/	N/	37
	O		-	O-	168
	P		.	P.	75

* D_T = Transformed Divergence
(Ranges from 0 to 2000)

PRINCIPAL COMPONENT ANALYSIS

Comparison of A and P-Tape MSS Results

As shown in Tables 5 and 6 the statistics generated from every fifth line and fifth column from the same area in the Chicago frame for both the A and P tapes are essentially identical. In addition, the resulting eigenvalues and eigenvectors from these statistics (i.e. covariance matrices) are also identical. This further corroborates the fact that the A and P tapes are radiometrically identical and that the cubic convolution process had little effect on the radiometry of the data.

Comparison of TM and MSS P-Tape Results

A. Significant Dimensionality

One of the major advantages of using orthogonal linear transformations such as the Principal Component or Karhunen-Loeve transformation is in their ability to compress overall data variance in a multifeature space onto a relatively few number of transformed orthogonal axes. This essentially separates non-random variance (information content) from random variance (noise), while, concurrently, uncorrelating the transformed axes in such a way that any information redundancy (due to interband correlation) is eliminated. Such transformations therefore allow a compression of the data into a fewer number of dimensions while retaining a maximum amount of significant information content and removing much of the random variance or noise from the data.

Principal components were generated for this part of the analysis for both the MSS and TM P-Tape data sets from the Chicago O'Hare test site. Figs. 1 through 4 show the images of the Landsat MSS four spectral bands of the Chicago O'Hare test site, and Figs. 5 through 8 show the Landsat MSS four ordered principal components of this test site. Also, Figs. 9 through 15 show the images of the Landsat TM seven spectral bands of the Chicago O'Hare test site, and Figs. 16 through 22 show the seven ordered principal components of this test site. Statistics used in calculating these principal components were generated from data samples of the original MSS and TM data sets from every fifth line and fifth column. Tables 6 and 7 show the statistics for the MSS and TM data sets, respectively. Since the sum of the eigenvalues is equal to the trace of the original covariance matrix, i.e. the total variance, the importance or percent of total variance explained by eigenvector(λ_i) is given by:

$$\frac{\alpha_i}{\text{tr } S}$$

where

α_i = eigenvalue i or characteristic root of the ith component

tr S = trace of covariance matrix S or total variance.

Table 5.

STATISTICS FOR THE MSS 'A' TAPE
FOR THE CHICAGO O'HARE TEST SITE
(Scene ID: 40101-10625)

Covariance Matrix Diagonal

16.7	29.6	32.1	23.7

Correlation Matrix

1.00			
0.92	1.00		
0.56	0.55	1.00	
0.15	0.13	0.82	1.00

Table 6.

STATISTICS FOR THE MSS 'P'TAPE
FOR THE CHICAGO O'HARE TEST SITE

Covariance Matrix Diagonal

17.5	30.0	32.4	25.5

Correlation Matrix

1.00			
0.93	1.00		
0.54	0.53	1.00	
0.11	0.11	0.83	1.00

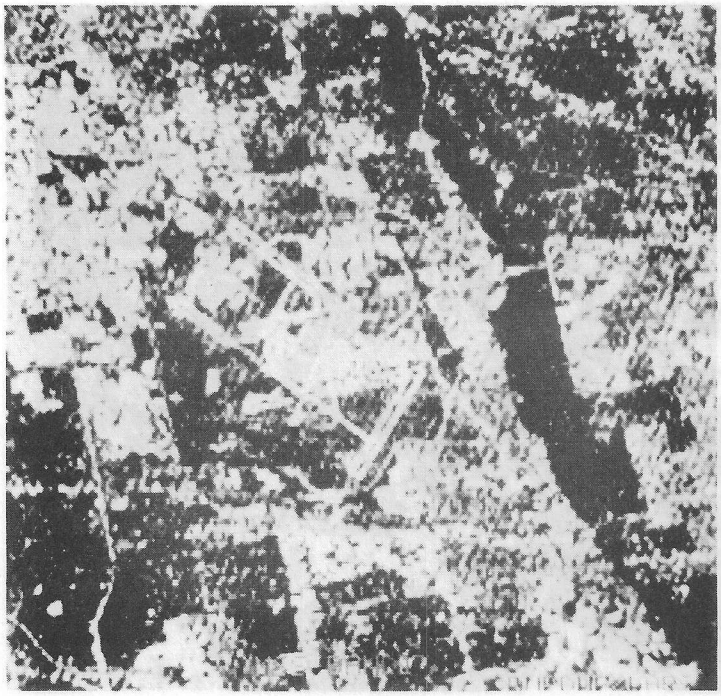

Fig. 1 Image of Band 1 (0.50 - 0.60μm) of Landsat IV MSS of the Chicago O'Hare Test Site.

Fig. 2 Image of Band 2 (0.60 - 0.70μm) of Landsat IV MSS of the Chicago O'Hare Test Site.

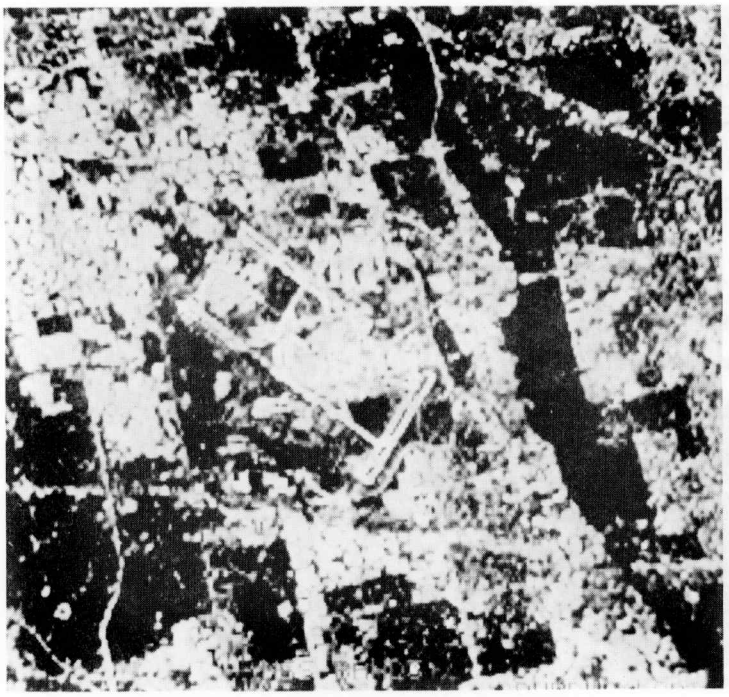

Fig. 3 Image of Band 3 (0.70 - 0.80μm) of Landsat IV MSS of the Chicago O'Hare Test Site.

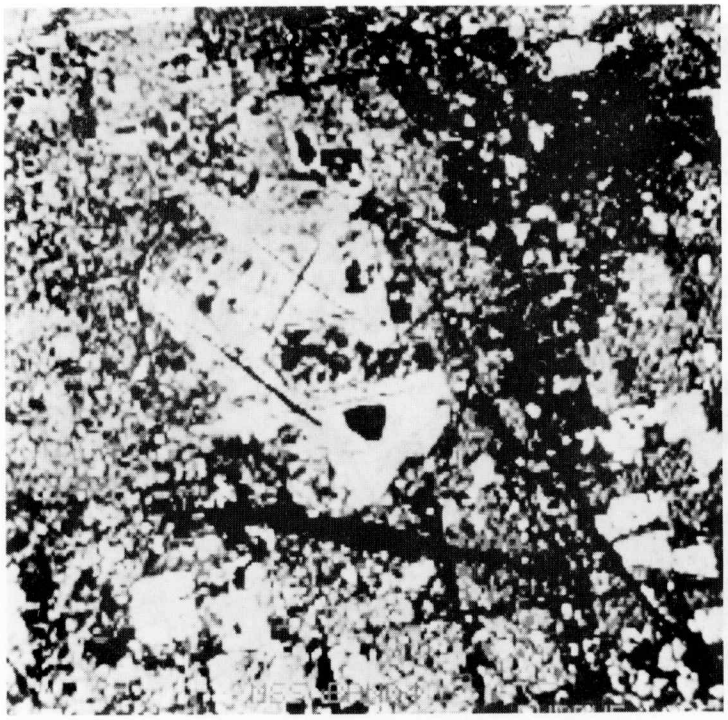

Fig. 4 Image of Band 4 (0.80 - 1.10μm) of Landsat IV MSS of the Chicago O'Hare Test Site.

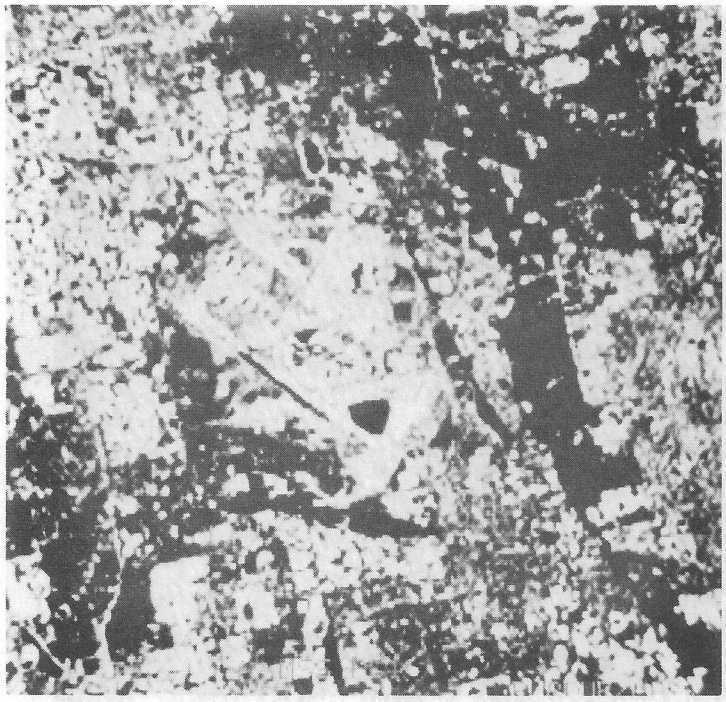

Fig. 5 Image of Principal Component 1 of Landsat IV MSS of the Chicago O'Hare Test Site.

Fig. 6 Image of Principal Component 2 of Landsat IV MSS of the Chicago O'Hare Test Site.

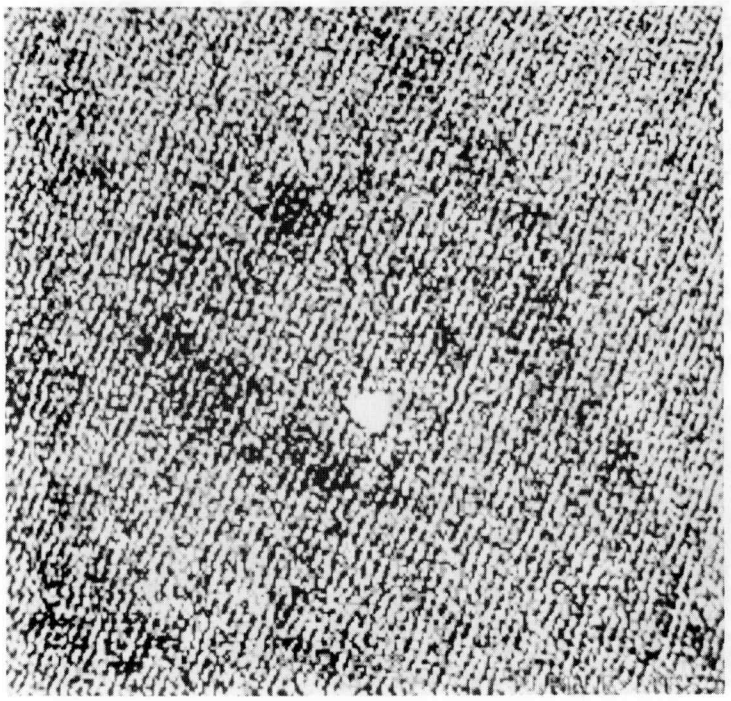

Fig. 7 Image of Principal Component 3 of Landsat IV MSS of the Chicago O'Hare Test Site.

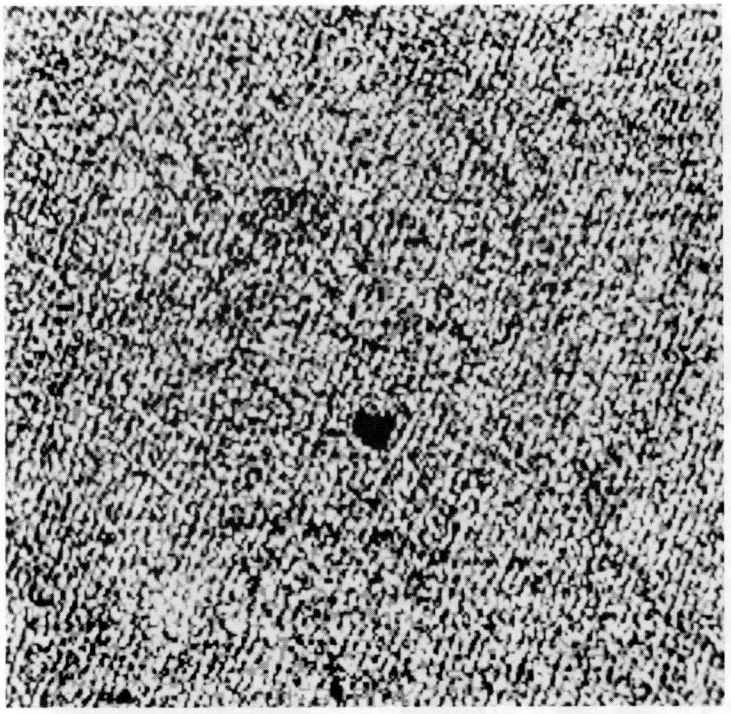

Fig. 8 Image of Principal Component 4 of Landsat IV MSS of the Chicago O'Hare Test Site.

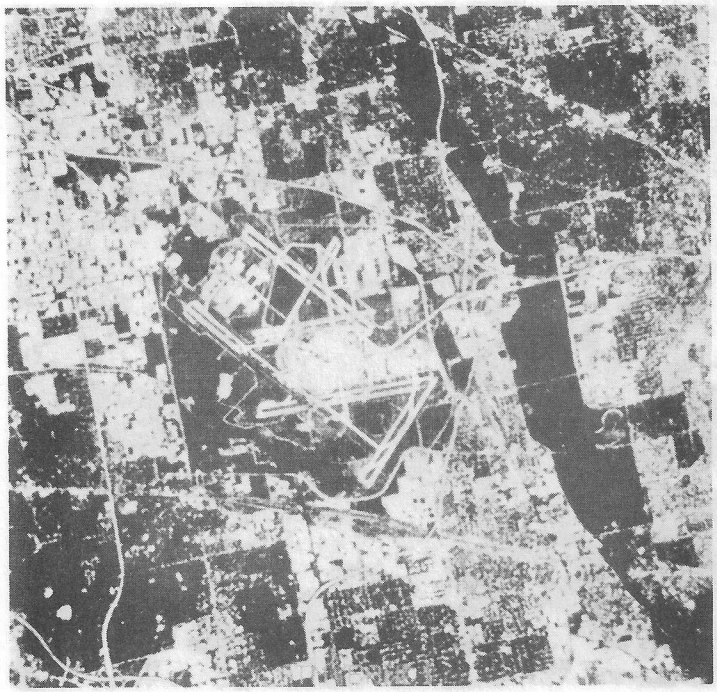

Fig. 9 Image of Band 1 (0.45 - 0.52μm) of Landsat IV TM of the Chicago O'Hare Test Site.

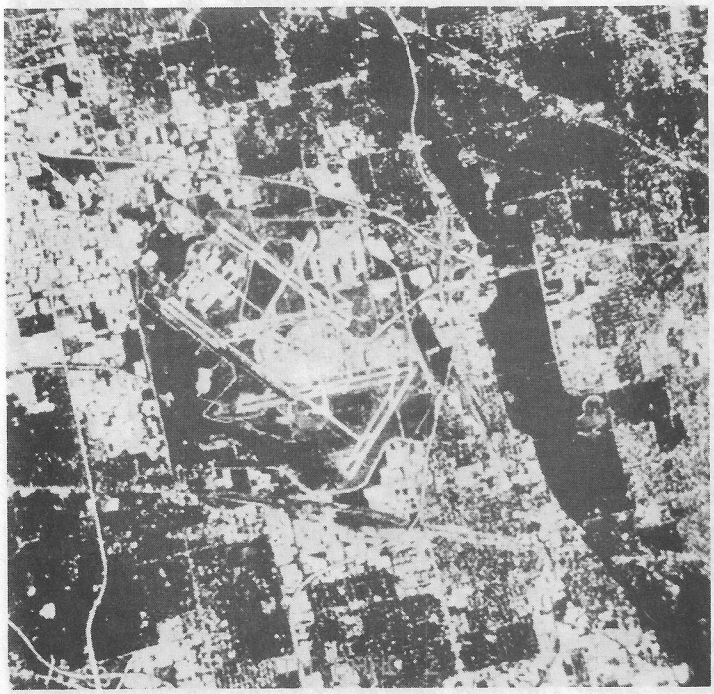

Fig. 10 Image of Band 2 (0.52 - 0.60μm) of Landsat IV TM of the Chicago O'Hare Test Site.

Fig. 11 Image of Band 3 (0.63 - 0.69μm) of Landsat IV TM of the Chicago O'Hare Test Site.

Fig. 12 Image of Band 4 (0.76 - 0.90μm) of Landsat IV TM of the Chicago O'Hare Test Site.

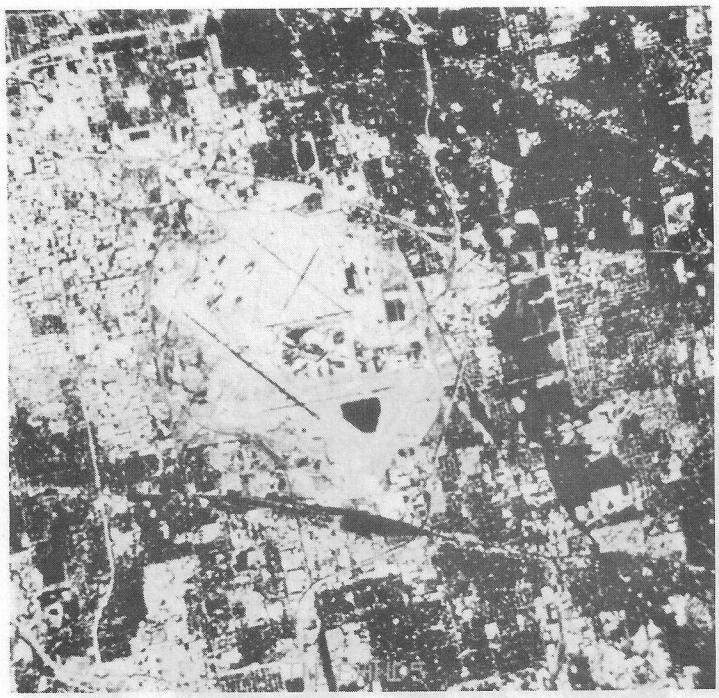

Fig. 13 Image of Band 5 (1.55 - 1.75μm) of Landsat IV TM of the Chicago O'Hare Test Site.

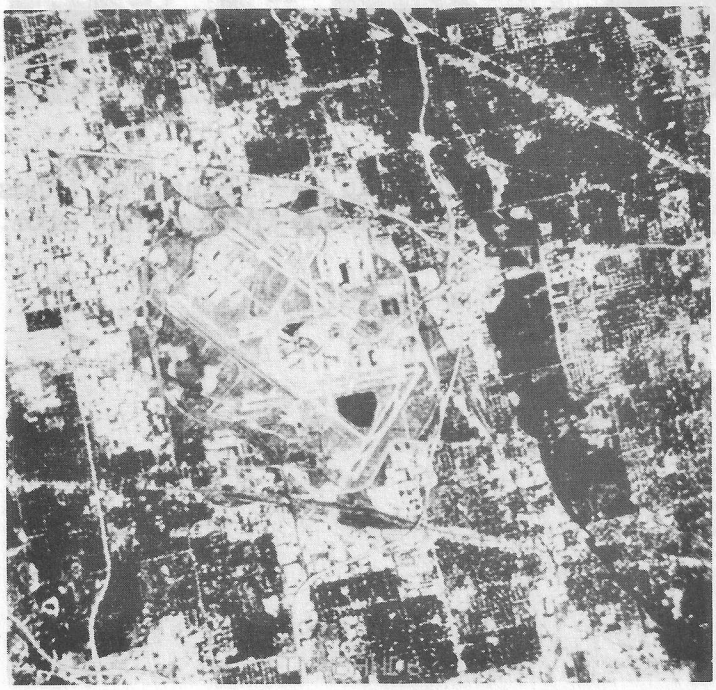

Fig. 14 Image of Band 6 (2.08 - 2.35μm) of Landsat IV TM of the Chicago O'Hare Test Site.

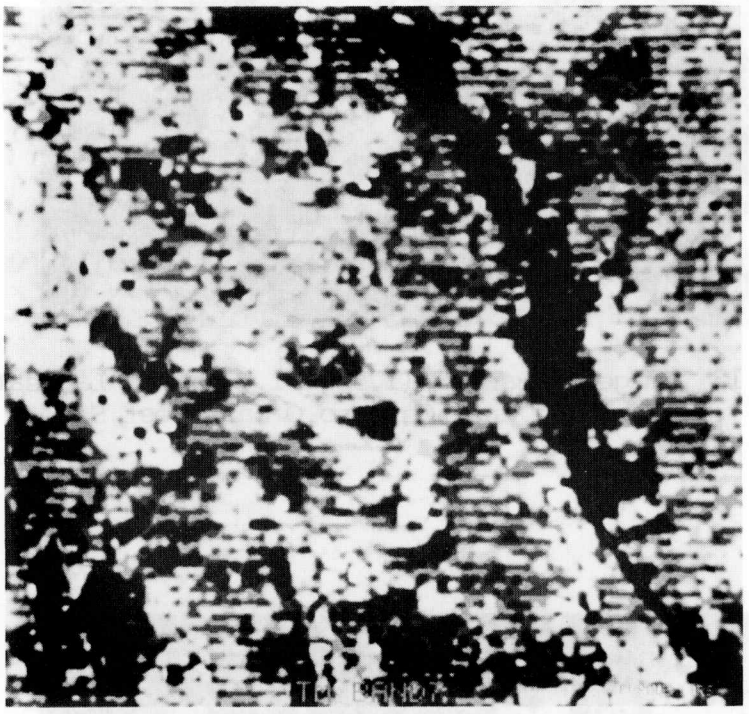

Fig. 15 Image of Band 7 (10.4 - 12.5μm) of Landsat IV TM of the Chicago O'Hare Test Site.

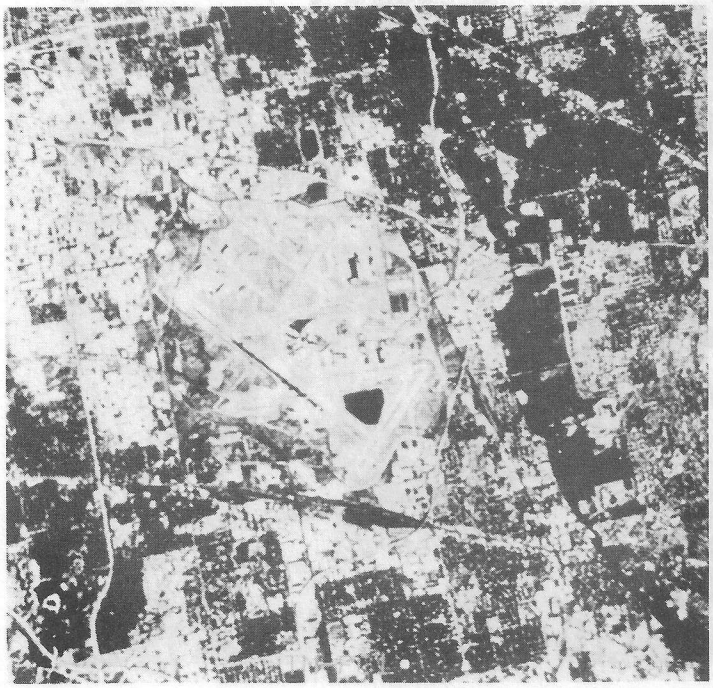

Fig. 16 Image of Principal Component 1 of Landsat IV TM of the Chicago O'Hare Test Site.

Fig. 17 Image of Principal Component 2 of Landsat IV TM of the Chicago O'Hare Test Site.

Fig. 18 Image of Principal Component 3 of Landsat IV TM of the Chicago O'Hare Test Site.

Fig. 19 Image of Principal Component 4 of Landsat IV TM of the Chicago O'Hare Test Site.

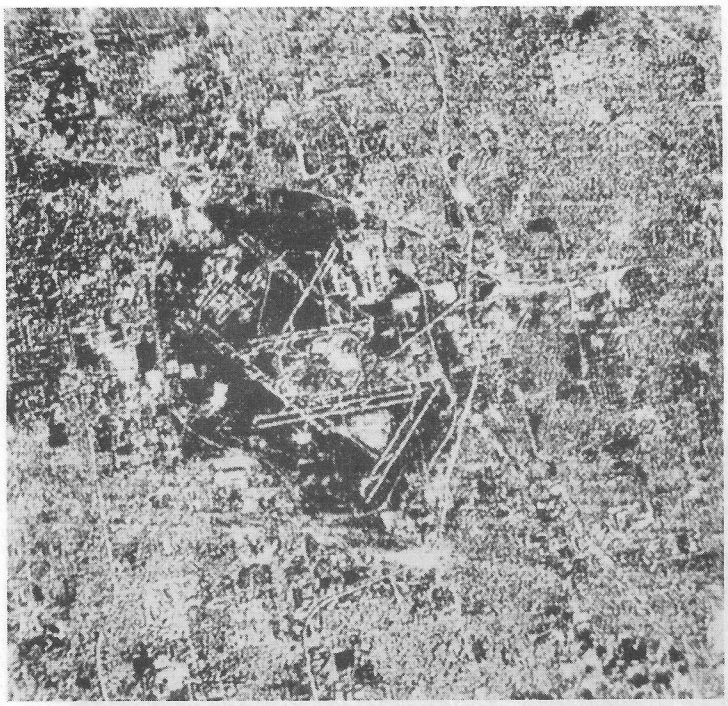

Fig. 20 Image of Principal Component 5 of Landsat IV TM of the Chicago O'Hare Test Site.

Fig. 21 Image of Principal Component 6 of Landsat IV TM of the Chicago O'Hare Test Site.

Fig. 22 Image of Principal Component 7 of Landsat IV TM of the Chicago O'Hare Test Site.

Table 7

STATISTICS FOR THE TM 'P' TAPE
FOR THE CHICAGO O'HARE TEST SITE
(Scene ID: 40101-16025)

Covariance Matrix Diagonal

90.9	35.6	72.5	80.5	194.5	80.1	6.7

Correlation Matrix

1.00						
0.96	1.00					
0.96	0.97	1.00				
0.19	0.27	0.24	1.00			
0.54	0.62	0.65	0.59	1.00		
0.77	0.82	0.85	0.30	0.86	1.00	
0.34	0.36	0.35	0.15	0.30	0.36	1.00

Therefore, each of the eigenvalues of the ordered components divided by the sum of the eigenvalues represents the amount of total data variance or information content accounted for by each eigenvector. Tables 8 and 9 list the eigenvalues and the corresponding amount of data variance that is accounted for by their respective eigenvectors, for both the MSS and the TM data sets. As shown in these tables, the first two principal components of the MSS P-tape account for almost 97% of the total data variance. This is also evident from the images of the ordered MSS principal components. The first two components contain a significant amount of scene contrast and data structure, while the last two MSS components contain mostly random noise.

In the TM data set, the first two ordered components together account for 90% of the data variance, the first three account for 97.45% and the first four components almost 99% of the data variance. The images of the TM principal components again show that the first four components contain a significant amount of scene contrast with a sequential decrease in this scene contrast in the lower ordered components. Figs. 23 and 24 graphically show the percent variance of the ordered components. From these it is readily apparent that a significant amount of the variance is accounted for by the first ordered principal components.

From both the listed eigenvalues and the images of the ordered components of the MSS and TM data sets, it is possible to conclude that the first two components of the MSS and the first four components of the TM data sets contain a maximum amount of significant information. It could be

possible, therefore, to conclude that for this data set of the Chicago O'Hare area, the TM data contains more significant information, i.e. a higher significant dimensionality, than the corresponding MSS data set. The significant dimensionalities as defined by a principal component analysis may be substantially different for other data sets and other ground cover types. However, these results do imply that for the same area, the TM may contain more significant information than the corresponding MSS.

Table 8.

TABLE OF EIGENVECTORS (PRINCIPAL COMPONENTS) AND EIGENVALUES OF THE MSS 'P' TAPE DATA FOR THE CHICAGO O'HARE TEST SITE (Scene ID: 40101-10625)

Matrix of Eigenvectors

	Principal Component (Eigenvector)			
Wavelength Band	1	2	3	4
1	0.39291	-0.41975	0.36717	0.73117
2	0.51763	-0.57144	-0.54223	-0.33392
3	0.64029	0.31652	0.54675	-0.43693
4	0.40951	0.63015	-0.52176	0.40371

Eigenvector	Eigenvalue	Percent Variance	Cumulative Percentage
1	68.83	65.30%	65.30%
2	33.18	31.48%	96.78%
3	1.98	1.88%	98.66%
4	1.42	1.34%	100.00%

B. Comparison of Principal Component Loadings

It is possible to qualitatively describe the relative importance of the original variables (spectral bands) to a particular eigenvector using their respective coefficients, as long as the original variables are fairly commensurable, such as is the case with both the MSS and the TM spectral bands. In this situation, the larger the coefficient of a given variable, the more importance or weight that variable is given in that particular eigenvector. The coefficients are sometimes referred to as 'loadings' and can be used to describe qualitatively the relative importance of the original bands to the data set in general. This is especially true with the higher ordered eigenvectors which contain most of the important information; i.e. it can be inferred that those variables or spectral bands which have relatively high coefficients in one or more of the first ordered components, are also more important in the original data set.

Tables 25 and 26 show graphically the coefficients or loadings of the original bands of the MSS and the TM data sets in each of the ordered eigenvectors or principal components. The first eigenvector or component of the TM shows a relatively high weighting of band 5 and, to a lesser degree, of band 6. This may be due to the relatively high correlation between bands 5 and 6 (Table 7) rather than a significant amount of contribution from both. Pictorially the importance of band 5 can be observed in the first Principal Component image when compared with the original image of band 5. Furthermore, band 5 was consistently selected by a transformed divergence (spectral separability) criterion as being the best single band for separating 12, 16, and 20 cluster classes of the Chicago O'Hare test area. It is interesting to note that component 4, although it accounts for only about 1% of the data variance (Table 9), its image shows that it still has clearly recognizable image content. In this case, the thermal band has the highest loading on component 4 which is readily apparent from a comparison of the two images, i.e. component 4 and the original band 7 (thermal IR). It is also important to note that the information content of the principal component 4 is strikingly similar to the thermal IR image, but it shows a higher spatial resolution. This is probably a result of the contributions from the other reflective bands of higher spatial resolution.

C. Scaling Effects

Since the Principal Component transformation is a linear orthogonal transformation which constructs a new set of uncorrelated axes from an original set of correlated axes. It constructs the new variables from the eigenvectors and eigenvalues of either a variance-covariance matrix or a correlation matrix. The new axes have directions as determined by the ordered eigenvectors of this matrix with length proportional to the square root of their respective eigenvalues. In multidimensional space, such transformations will not alter the Euclidean distance between data points (Ref. 8). However, if the resulting components are given some relative magnitude or length other than values which are proportional to the square roots of their respective eigenvalues, then the Euclidean distance between data points will be altered. Clustering algorithms are often highly sensitive to such movements or changes in position of data points with respect to each other. Therefore, it is important for clustering and classification purposes that the resulting transformed components of such

Table 9

TABLE OF EIGENVECTORS (PRINCIPAL COMPONENTS) AND EIGENVALUES
OF THE TM "P" TAPE DATA FOR THE CHICAGO O'HARE TEST SITE
(Scene ID: 40101-10625)

	Principal Component (Eigenvector)						
	1	2	3	4	5	6	7
Wavelength Band							
1	0.38933	-0.48411	0.33460	-0.10358	-0.21253	-0.66554	-0.05709
2	0.25827	-0.24404	0.18937	-0.00917	-0.02399	0.36076	0.84078
3	0.37575	-0.35741	0.17324	-0.06512	-0.05095	0.63914	-0.53453
4	0.23126	0.59933	0.72770	0.07013	0.22440	-0.01326	-0.04812
5	0.63867	0.45624	-0.43559	-0.15732	-0.40970	-0.02462	0.03150
6	0.42059	-0.10269	-0.32059	0.25366	0.79236	-0.13257	-0.00453
7	0.04739	-0.02105	0.00999	0.94389	-0.32497	0.00707	-0.02493

Eigenvector	Eigenvalue	Percent Variance	Cumulative Percentage
1	402.90	71.84%	71.84%
2	102.29	18.24%	90.07%
3	41.37	7.38%	97.45%
4	5.90	1.05%	98.50%
5	4.96	0.88%	99.39%
6	2.20	0.39%	99.78%
7	1.24	0.22%	100.00%

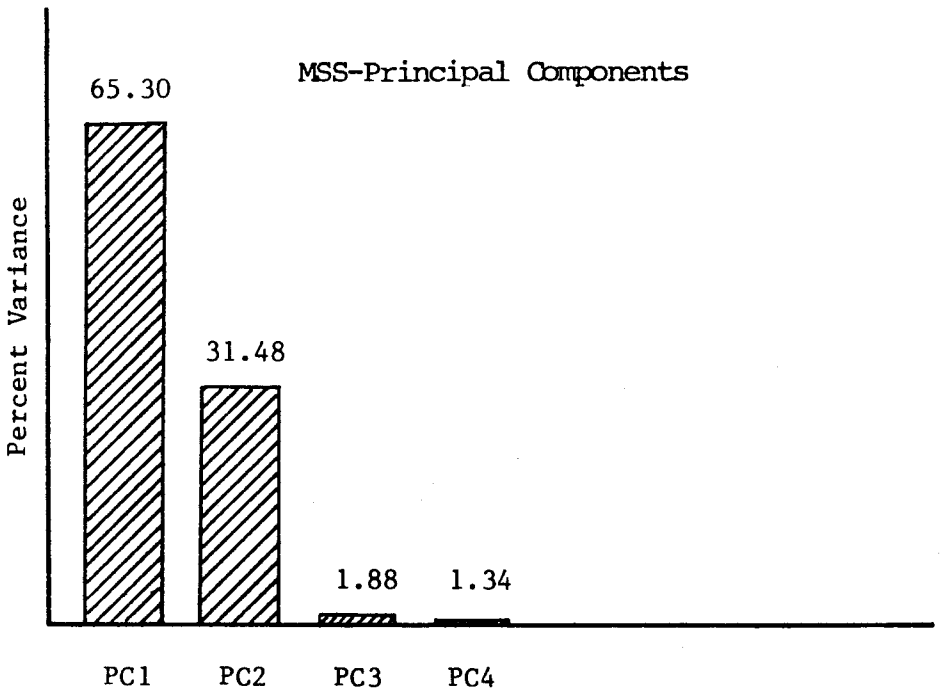

Fig. 23 Percent of Total Data Variance Accounted for by Each of the Ordered MSS Principal Components.

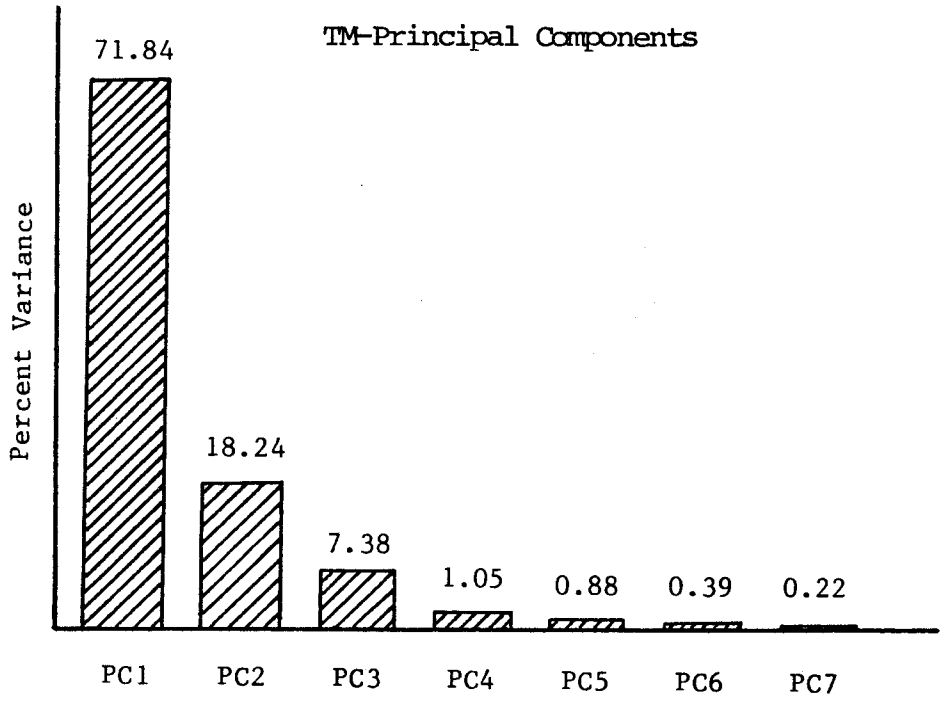

Fig. 24 Percent of Total Data Variance Accounted for by Each of the Ordered TM Principal Components.

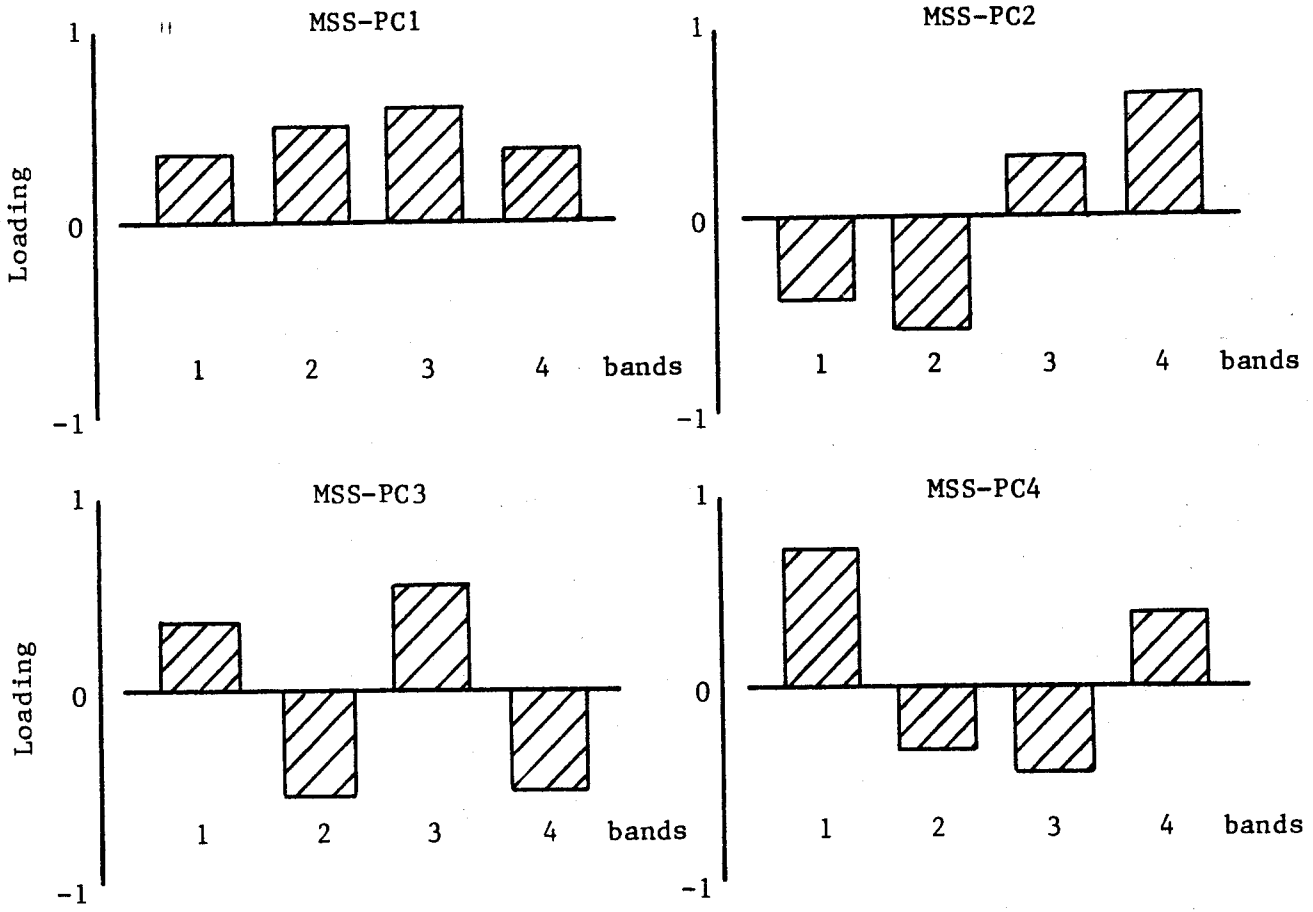

Fig. 25 The Loadings or Coefficients of the Original Wavelength Bands on Each of the Ordered MSS Principal Components.

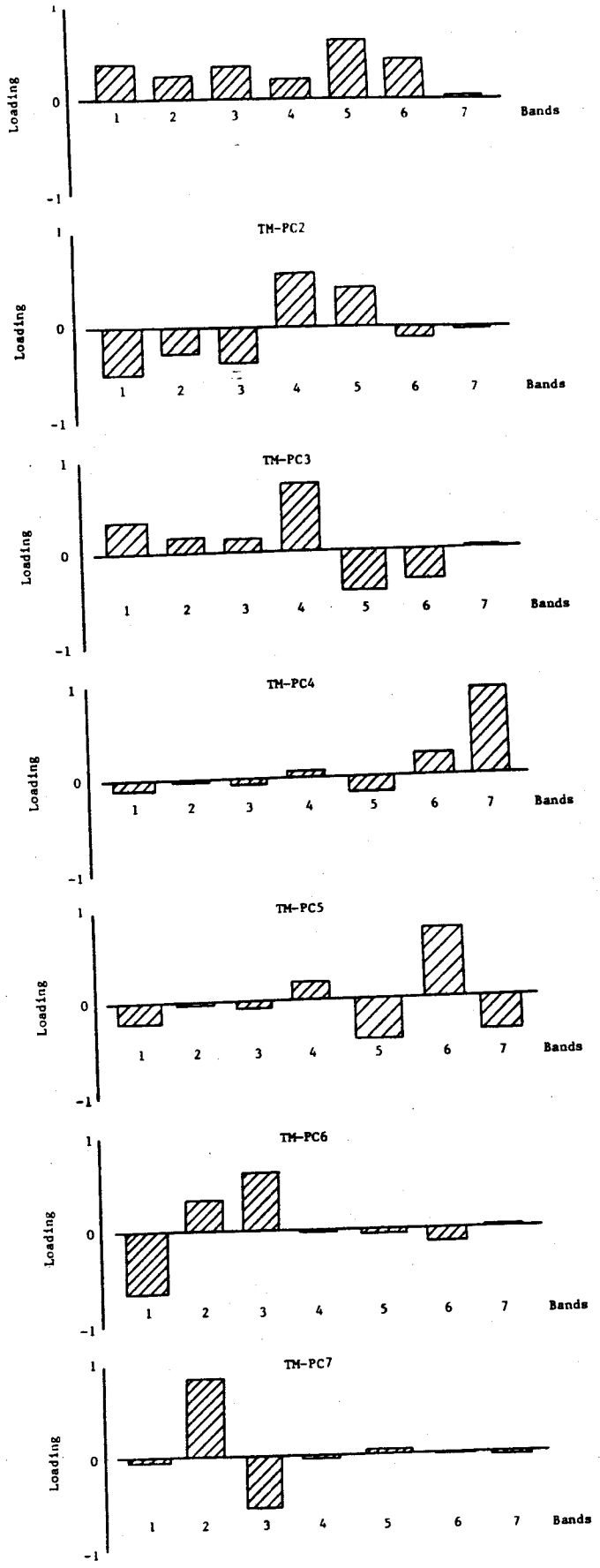

Fig. 26 The Loadings or Coefficients of the Original Wavelength Bands on Each of the Ordered TM Principal Components.

orthogonal transformations be correctly scaled. Previous experience has demonstrated little or no correlation between cluster classes from an incorrectly, e.g. contrast stretched, principal component data set with actual spectral clusters of the original, untransformed data.

D. Clustering of the Original and Transformed TM data

Both the original and a Principal Component transformed TM P-tape data set from the Chicago O'Hare test site were each clustered separately into 16 cluster classes. With the original TM data all 7 bands were used for clustering while for the transformed data set, three unique sets of 16 clusters were generated using only the first three, four and all seven components, respectively. Both a minimum transformed divergence value (D_T(Min)) and an average transformed divergence value (D_T(Ave)) for each waveband and principal component set are given in Tables 10 and 11.

Table 10.

SEPARABILITY OF 16 CLUSTER CLASSES FOR THE 'BEST' TWO AND MORE WAVELENGTH BAND COMBINATIONS OF THE TM DATA FROM THE CHICAGO O'HARE TEST SITE (Scene ID: 40101-16025)

Wavelength Band Combination	D_T(Min)	D_T(Ave)
(3,5)	68	1859
(3,4,5)	1281	1929
(3,4,5,6)	1312	1937
(1,3,4,5,6)	1322	1944
(1,3,4,5,6,7)	1347	1947
(1,2,3,4,5,6,7)	1361	1950

Table 11.

SEPARABILITY OF 16 CLUSTER CLASSES FOR THE COMBINATIONS OF THE FIRST 3,4 AND ALL 7 ORDERED PRINCIPAL COMPONENTS OF THE TM DATA FROM THE CHICAGO O'HARE TEST SITE (Scene ID: 40101-16025)

Principal Components	D_T(Min)	D_T(Ave)
(1,2,3)	1261	1934
(1,2,3,4)	1257	1934
(1,2,3,4,5,6,7)	1322	1946

The clusters produced from the 7 bands of the original data set were very similar to those produced from the 7 components of the transformed data. Furthermore, the clusters generated from the first three and the first four principal components were almost identical to those generated from the 7 components. Both the original and the transformed data set separabilities indicate that a dimensionality of three is required for optimum separability with little increase in separability beyond three dimensions. These results indicate that identical cluster groupings are likely to be obtained with a subset of the higher ordered components as those obtained with all 7 components and using a fraction of the computer time. Three components in this case produced an optimum cluster grouping using only 1/3 of the CPU time required for clustering with all 7 components.

TEMPERATURE MAPPING OF A COOLING POND AND THERMAL PLUME FROM A NUCLEAR POWER PLANT

The use of thermal infrared (IR) data in conjunction with reflective multispectral data, obtained from aircraft altitudes, has been proven to be an effective means for increasing the classification accuracy of earth surface features (Ref.s 7, and 11).

Also it has been demonstrated that radiometrically calibrated thermal IR data obtained from airborne platforms can be used to produce accurate temperature maps of water bodies (Ref.s 1,3,4, and 10).

Accurate temperature maps of water bodies have been obtained also from calibrated thermal IR data gathered in 1973 by the SKYLAB SL-2 S192 scanner system (Ref. 6). However, for almost ten years the remote sensing data users have not had available high spatial resolution thermal IR data (in contrast to the coarse spatial resolution data gathered by meteorological satellites) acquired from spaceborne platforms, until the TM thermal data were recently collected.

In order to determine the radiometric quality of the TM thermal data for temperature mapping of surface water, a test site was selected within the area covered by the TM scene (Scene ID: 40101-16025) gathered over Illinois. This site was chosen because it includes a surface water body with a large range of temperatures, i.e. a cooling pond for the Dresden nuclear power plant and the junction of two rivers: the Kankakee and the Des Plaines rivers which once merged form the Illinois river.

The Dresden power generating station is located approximately 50 miles southwest of Chicago near Morris, Illinois. The station houses three nuclear reactors which together have a maximum nameplate generating capacity of 1,656,630 Kw. The water which is taken from the Kankakee river and is used to cool the steam condensers is channeled into a man-made lake which is designed to dissipate heat. This 1300 acre lake has a dike in its center which directs the water flow up, around and down the lake in an eight-mile loop that takes two-and-a-half days to complete. During its

course the water is cooled by natural evaporation and is either recycled back through the station or discharged into the Illinois river. A schematic diagram of the power plant, channels, cooling lake, and the three rivers is shown in Fig. 27.

Because the radiant temperature of the various cover types in the test site is a function not only of the kinetic temperature of the materials, but it is also a function of the intrinsic emissive properties (emissivity) of the objects, and to avoid differential emissivity complications, it was decided to perform the calibration of the TM thermal IR data corresponding to only those pixels representing water, which has an emissivity close to that of a perfect radiator or blackbody.

To accomplish the thermal calibration of water only, a heirarchical classification of the TM data had to be performed, i.e. one of the middle IR (1.55 - 1.75 μm) band was utilized to discriminate the water pixels from all the other cover types using the LARSYS layered classifier (Ref.s 3,5,15), and once all the water pixels were separated from everything else, their thermal IR response (relative digital count) was converted to radiant temperatures. Fig. 28 shows the decision tree utilized to carry out the heirarchical or layered classification and calibration of the water bodies present in the test site, and Figs. 29 and 30 show the images of the test site corresponding to the 1.55-1.75μm and 10.4-12.5μm bands respectively.

The conversion of the relative thermal IR responses into radiant temperature measurements was accomplished using a 'non-linear' calibration function derived specifically for the TM thermal IR band and the range of temperatures of the two internal calibration reference blackbodies.

The 'non-linear' calibration function was derived through the integration of Planck's equation for a spectral band covering the 10.4-12.5μm spectral range, and for a range of temperatures between 260 K and 320 K (Ref. 2) at increments of 0.1 K. The resulting in-band radiances (in Watts/cm^2-sr) were then plotted versus the corresponding temperatures as illustrated in Fig. 31. Note in this figure that if one assumes a linear relationship between the emitted energy from a blackbody and its temperature for a range of temperatures in excess of 10 K (the range between the cold and hot internal calibration sources of the TM system is 60 K), errors on the order of 4 K (4°C) would be introduced.

The non-linear calibration function is given by Equation 1 below:

$$T(^\circ C) = -12.5809 + 0.2917D - 0.000233D^2 \qquad (1)$$

where: T = temperature in degrees Celsius
D = relative digital counts for the TM thermal IR band

If a linear interpolation was performed, the linear calibration function would be represented by Equation 2:

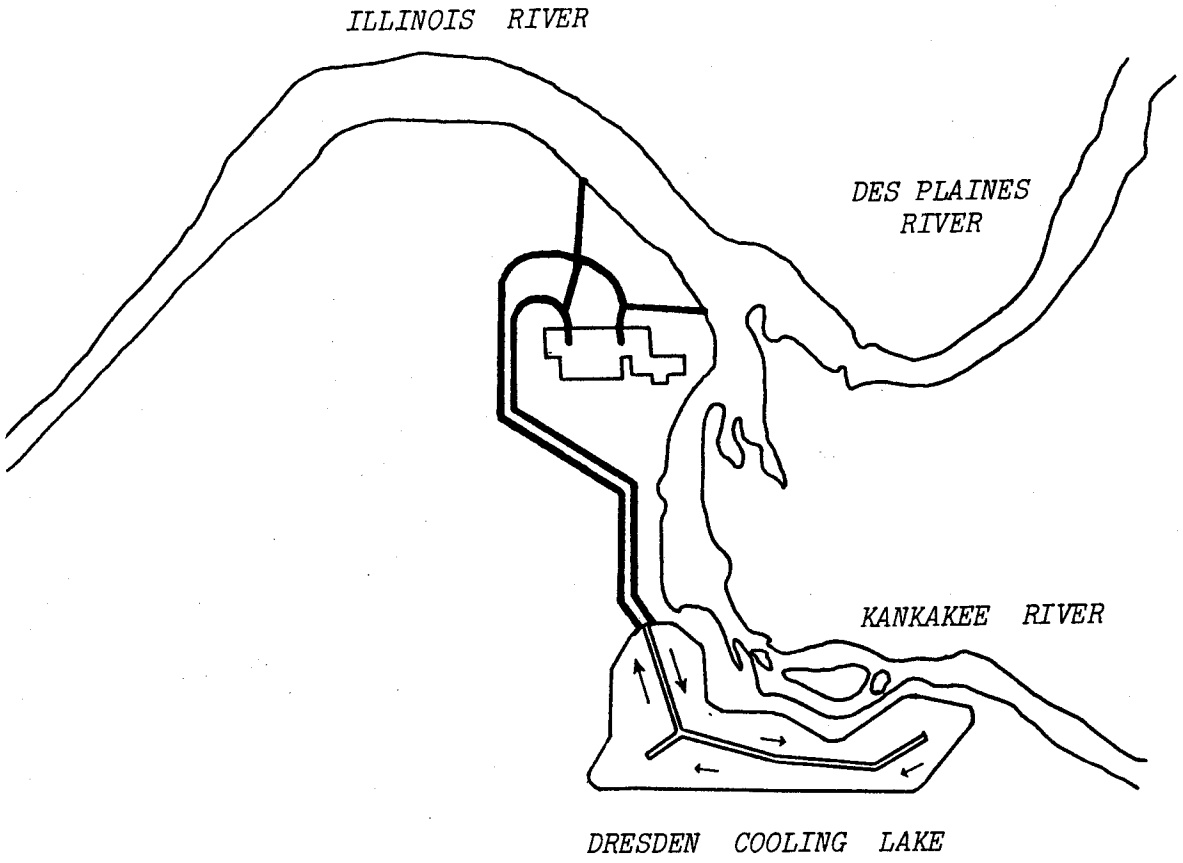

Fig. 27 Schematic Diagram of the Dresden Nuclear Power Plant, Channels, Cooling Lake and the Kankakee, Des Plaines and Illionois Rivers.

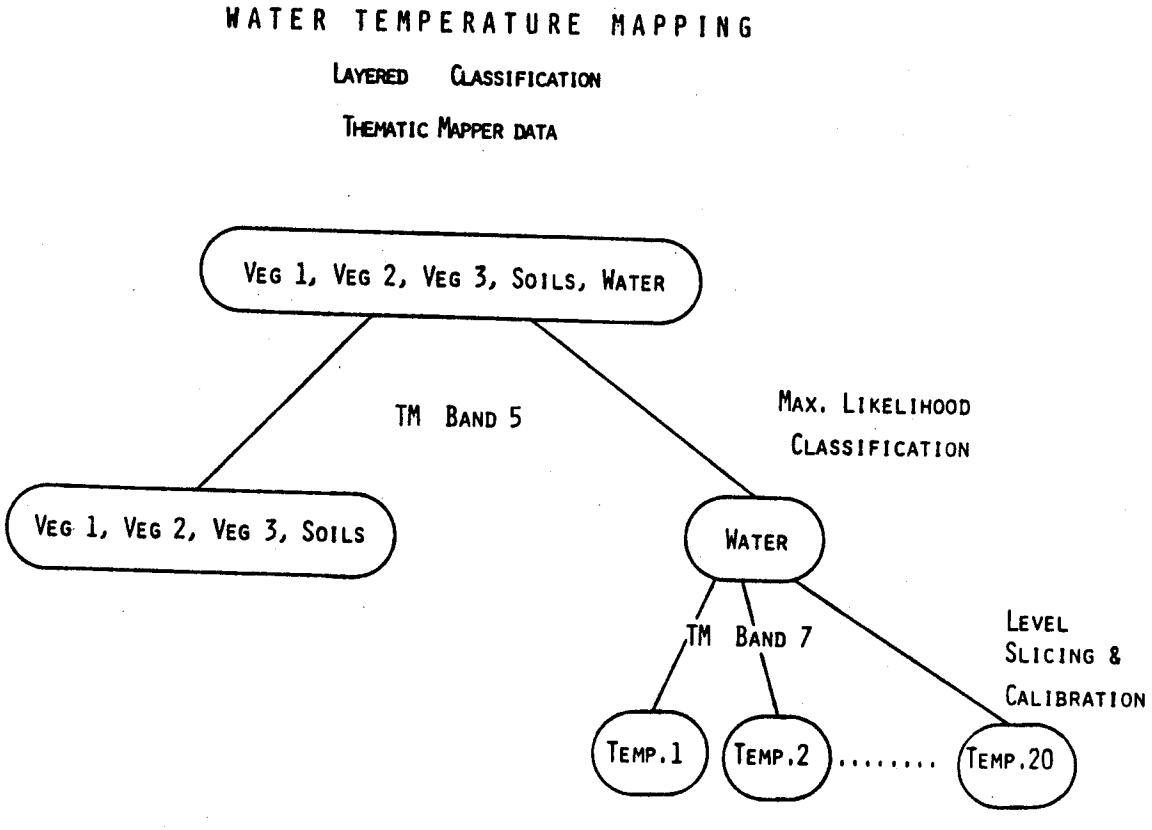

Fig. 28 Decision Tree Utilized to Carry out the Heirarchical Classification and Calibration of the Water Bodies Present in the Dresden Nuclear Power Plant Test Site.

Fig. 29 Image of Band 5 (1.55 - 1.75μm) of Landsat IV TM of the Dresden Power Plant Test Site.

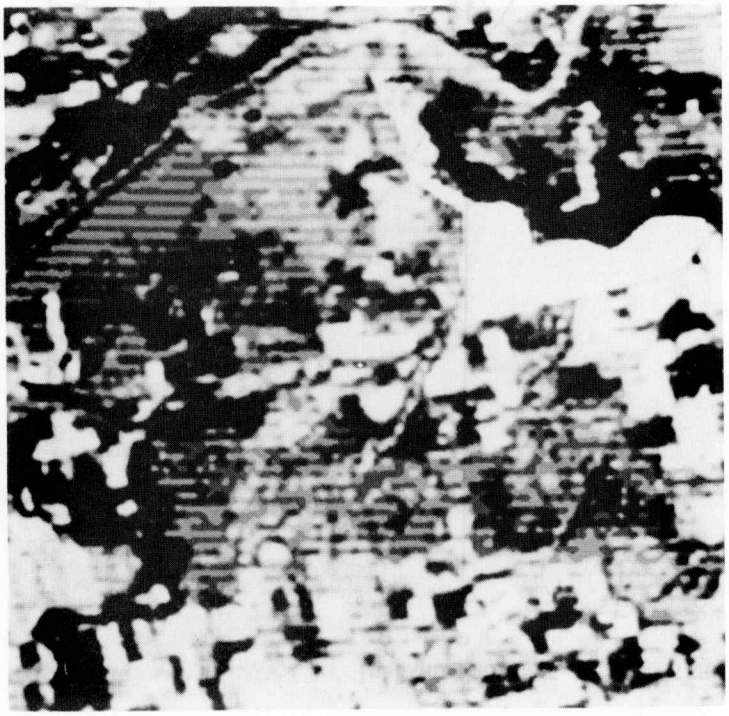

Fig. 30 Image of Band 7 (10.4 - 12.5μm) of Landsat IV TM of the Dresden Power Plant Test Site.

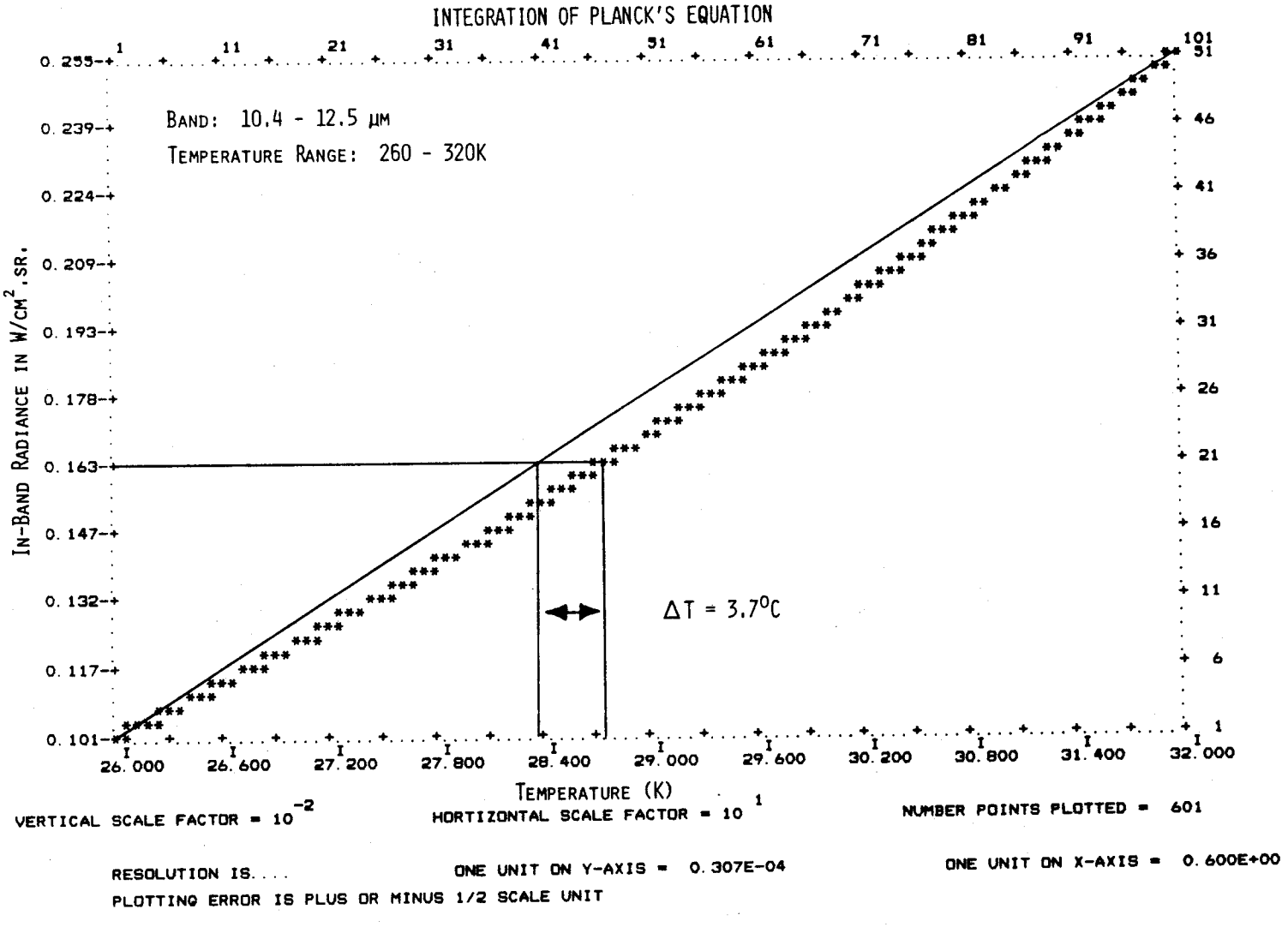

Fig. 31 Integration of Planck's Equation for a Spectral Band Covering the 10.4 - 12.5µm Spectral Range, and for a Range of Temperatures Between 260°K and 320°K at 0.1°K increments.

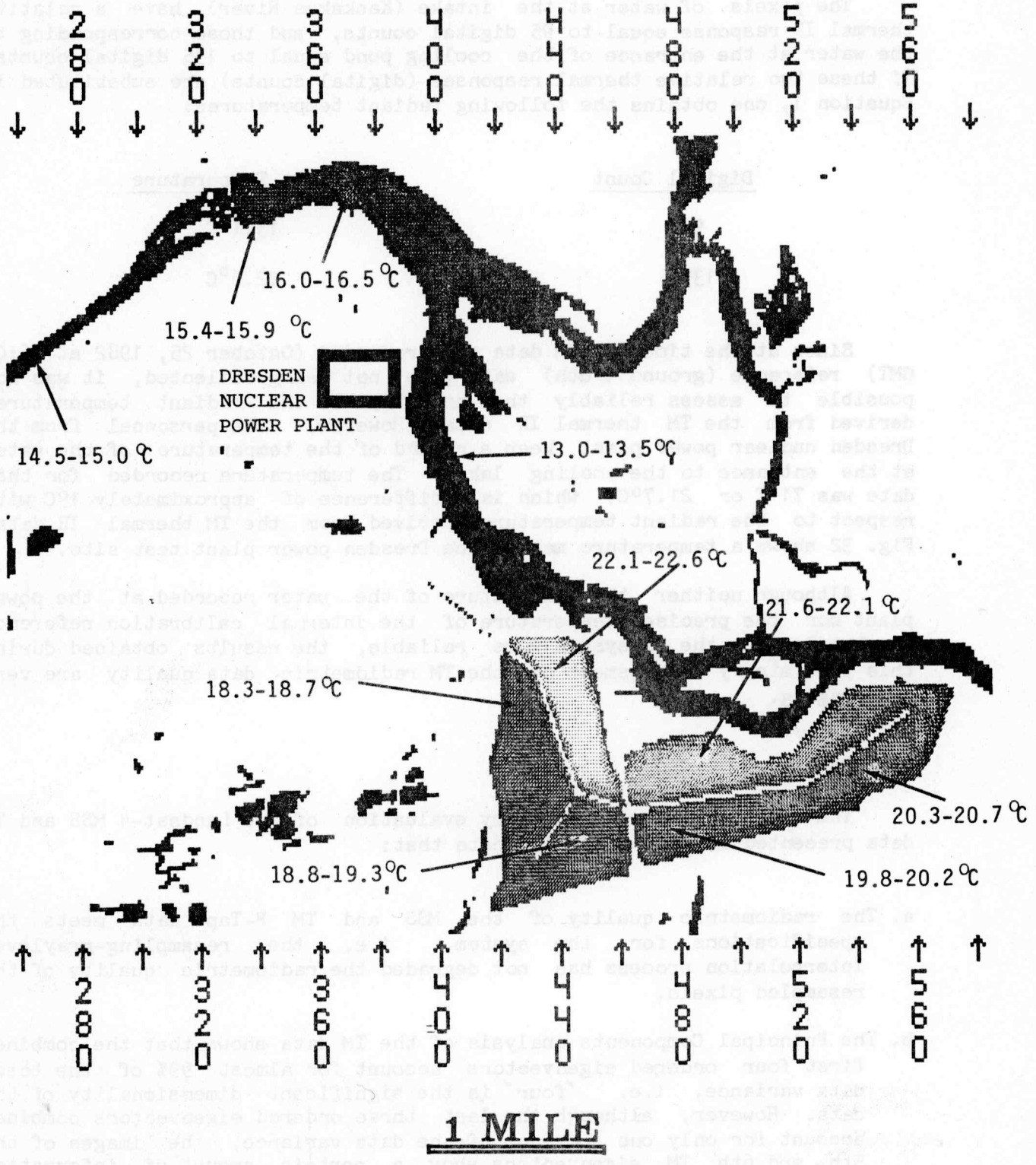

Fig. 32 Temperature Map of the Dresden Nuclear Power Plant Test Site Derived from the Landsat-4 TM Data.

$$T(^{o}C) = -13 + 0.23529D \quad (2)$$

The pixels of water at the intake (Kankakee River) have a relative thermal IR response equal to 95 digital counts, and those corresponding to the water at the entrance of the cooling pond equal to 135 digital counts. If these two relative thermal responses (digital counts) are substituted in Equation 1, one obtains the following radiant temperatures:

Digital Count	Radiant Temperature
95	13.1°C
135	22.6°C

Since at the time the TM data were recorded (October 25, 1982 at 16:02 GMT) reference (ground truth) data were not being collected, it was not possible to assess reliably the accuracy of the radiant temperatures derived from the TM thermal IR data. However, the personnel from the Dresden nuclear power plant keep a record of the temperature of the water at the entrance to the cooling lake. The temperature recorded for that date was 71°F or 21.7°C, which is a difference of approximately 1°C with respect to the radiant temperature derived from the TM thermal IR data. Fig. 32 shows a temperature map of the Dresden power plant test site.

Although neither the temperature of the water recorded at the power plant nor the precise temperature of the internal calibration reference blackbodies in the TM system were reliable, the results obtained during this preliminary assessment of the TM radiometric data quality are very encouraging.

CONCLUSIONS

The results of the preliminary evaluation of the Landsat-4 MSS and TM data presented in this paper indicate that:

a. The radiometric quality of the MSS and TM P-Tape data meets the specifications for the system, i.e. the resampling-graylevel interpolation process has not degraded the radiometric quality of the resampled pixels.

b. The Principal Components analysis of the TM data shows that the combined first four ordered eigenvectors account for almost 99% of the total data variance, i.e. 'four' is the significant dimensionality of the data. However, although the last three ordered eigenvectors combined account for only one percent of the data variance, the images of the 5th and 6th TM eigenvectors show a certain amount of information content. These results are in contrast with these obtained from the MSS data, in which the images for the last two ordered MSS eigenvectors contain only random variations or noise.

c. The 4th ordered principal component (eigenvector 4) from the TM data is primarily loaded by information originating in the thermal IR band, as illustrated in Table 9 and the comparison of the images included in Figures 15 and 19. It is very interesting to note that the image of the 4th ordered TM principal component is extremely similar to that of the TM thermal IR band, but it contains also higher spatial resolution information than the original thermal IR band.

d. The TM thermal IR data, when properly processed, could be effectively utilized to produce temperature maps of water bodies.

REFERENCES

1. Atwell, B.H., R.B. MacDonald, and L.A. Bartolucci, 'Thermal Mapping of Streams from Airborn Radiometric Scanning," Water Resources Bulletin, Journal of the American Water Resources Association, Vol. &, No. 2, Urbana, Illinois, April 1971.

2. Barker, T.L., 'TM Sensor Description and Status,' First European Landsat-4 Workshop, ESA/EARTHNET Program, Frascati, Italy, November 1982.

3. Bartolucci, L.A., R.M. Hoffer, and T.R. West, 'Computer-Aided Processing of Remotely-Sensed Data for Temperature Mapping of Surface Water from Aircraft Altitudes,' LARS Information Note 042373, Laboratory for Applications of Remote Sensing, Purdue University, West Lafayette, Indiana, April 1973.

4. Bartolucci, L.A., R.M. Hoffer, and J.R. Gammon, 'Effects of Altitude and Wavelength Band Selection on Remote Measurements of Water Temperature,' Proceedings of the First PanAmerican Symposium on Remote Sensing, Panama City, Panama, May 1973.

5. Bartolucci, L.A., P.H. Swain, and C.L. Wu, 'Selective Radiant Temperature Mapping Using a Layered Classifier,' Journal of the IEEE Geoscience Electronics, Bol. GE-14, No. 2, April 1976. Also Available as LARS Information Note 111175, 1975.

6. Bartolucci, L.A., 'Hydrologic Features Survey,' Chapter 4, LARS Information Note 121275, Laboratory for Applications of Remote Sensing, Purdue University, West Lafayette, Indiana, 1975.

7. Bauer, M.E., P.H. Swain, R.P. Mroczynski, P.E. Anuta, and R.B. MacDonald, 'Detection of Southern Corn Leaf Blight by Remote Sensing Techniques,' Proceedings of the Seventh International Symposium on Remote Sensing of the Environment, Vol.1, May 17-21, 1971, pp.693-704.

8. Duda, R.O. and P.E. Hart, Pattern Classification and Scene Analysis, John Wiley and Sons, New York, 1973.

9. Goddard Space Flight Center Specifications for the Landsat-D System, Revision C, March 1981, Greenbelt, Maryland, pp:3-88.

10. Hoffer, R.M. and L.A. Bartolucci, 'Remote Sensing Techniques for Measurements of Water Temperature,' LARS Information Note 111671, Laboratory for Applications of Remote Sensing, Purdue University, West Lafayette, Indiana, 1971.

11. Kumar,R. and L.F. Silva, 'Emission and Reflectance from Healthy and Stressed Natural Targets with Computer Analysis of Spectroradiometric and Multispectral Scanner Data,' LARS Information Note 072473, Laboratory for Applications of Remote Sensing, Purdue University, West Lafayette, Indiana, July 1973.

12. Swain, P.H., T.V. Robertson, and A.G. Wacker, 'Comparison of the Divergence and B-Distance in Feature Selection,' LARS Information Note 020871, Laboratory for Applications of Remote Sensing, Purdue University, West Lafayette, Indiana, February 1971.

13. Swain, P.H. and R.C. King, 'Two Effective Feature Selection Criteria for Multispectral Remote Sensing,' LARS Information Note 042673, Laboratory for Applications of Remote Sensing, Purdue University, West Lafayette, Indiana, April 1973.

14. Wacker, A., 'A Cluster Approach to Finding Spatial Boundaries in Multispectral Imagery,' LARS Information Note 122969, Laboratory for Applications of Remote Sensing, Purdue University, West Lafayette, Indiana, December 1969.

15. Wu, C.L., D.A. Landgrebe, and P.H. Swain, 'The Decision Tree Approach to Classification,' LARS Information Note 090174, Laboratory for Applications of Remote Sensing, Purdue University, West lafayette, Indiana, September 1974.